Transformation of dense shelf water cascade to supercritical turbidity currents: Impact on seabed geomorphology and implication for climate change

Nan Wu[1*], Guangfa Zhong[1], Yakup Niyazi[2], Harya D. Nugraha[3], Michael J. Steventon[4],

[1]State Key Laboratory of Marine Geology, Tongji University, 1239 Siping Road, Shanghai, 200092, China
[2]Minderoo-UWA Deep-Sea Research Centre, School of Biological Sciences and UWA Oceans Institute, The University of Western Australia, Perth, WA 6009, Australia
[3]Center for Sustainable Geoscience, Universitas Pertamina, Jakarta, 12220, Indonesia
[4]Shell Research, Shell Centre, London, SE1 7NA, UK
[*]Email: nanwu@tongji.edu.cn

ABSTRACT

Dense shelf water cascades (DSWC) are ubiquitous on continental margins worldwide. They could transform into turbidity currents, shape the seabed physiography, and influence sediment, organic carbon, and pollutants that transfer from the shelf to the basin floor. However, there is still a lack of knowledge regarding how DSWC transforms into turbidity currents, and how DSWC interacts with the seabed. The Central Region of the offshore Gippsland Basin, located on the southeast Australian margin, is seasonally impacted by DSWC (named the Bass Cascade Current; BCC) formed in the Bass Strait. We observed complex seabed morphologies and highly diverse sedimentary processes in this area using high-resolution multibeam bathymetry, seismic reflection, and core description data. Observed sedimentary structures include sediment waves, erosional scours, cyclic steps, submarine channels, longitudinal furrows, submarine landslides and gullies. We ascribe this complexity to a dynamic interaction between BCC, and Westerly wind-associated Ekman transport flow, and strong waves. We found that the along-shelf transported BCC can interact with the submarine landslides and generate supercritical turbidity currents transporting downslope for more than 80 km. We reveal that climate change could significantly impact the seabed morphologies and sedimentation processes, by dictating the

strength and pathway of BCC and its generated supercritical turbidity currents. Therefore, the current transformation has critical implications for predicting how seabed geomorphology, sedimentation process, and occurrence of geohazards respond to changing oceanographic and climate conditions.

Keywords: Dense shelf water cascade, Bass Cascade Current, supercritical turbidity current, Gippsland Basin

INTRODUCTION

Along the continental shelves, seasonal evaporation during summer and cooling during winter can generate a cross-shelf density gradient that drives denser seawater transport seawards along the seabed (Ivanov et al., 2004). This process is defined as Dense Shelf Water Cascade (DSWC). The DSWC can travel more than 10,000 km along the coastline and descends down the slope to greater depths (more than 1000 m) (Ivanov et al., 2004; Canals et al., 2009; Mahjabin et al., 2020). The DSWC is a ubiquitous process that has been found in many shallow marine regions around the world (Figure 1A; Ivanov et al., 2004), and canyon heads are often the major conduits for the such process (Canals et al., 2009; Morrison et al., 2020). Once the DSWC is initiated, it sinks and overflows the shelf area under the influence of gravity, cascading downslope until it reaches its density equilibrium depth (also known as neutral density level; Figure 1B) (Canals et al., 2009). The DSWC can affect a large portion of the seabed, induce erosion and deposition, and generate bottom nepheloid layers (zone) that contain significant amounts of suspended sediments, thus triggering turbidity current (Figure 1B; Canals et al., 2006; Puig, 2017). It has proved to be an effective seabed-sculpting process and is capable of transporting sediment, organic carbon, marine pollutants and plastic litter from shallow marine to the deep ocean environments (Palanques et al., 2006; Canals et al., 2009). Despite the extensive existing literature, some important questions remain: i) how does along-shelf DSWC transform into downslope-flowing turbidity current? ii) How does DSWC shape the seabed geomorphology and influence sedimentary processes? and iii) Why could

DSWC spread and spill over a great distance accross the shelf and even reach the lower slope?

The offshore Gippsland Basin is dominated by a cool-water carbonate system located on SE Australia's passive margin (Figure 2A). It is one of Australia's most prolific hydrocarbon provinces, fisheries, and potential carbon storage, and holds a number of other potential marine resource applications (Rahmanian et al., 1990; Mitchell et al., 2007a; Mitchell et al., 2007b). The Central Region of the Gippsland Basin is one of the regions where seabed morphologies influenced by DSWC (named Bass Cascading Current) have been best documented (Godfrey et al., 1980; Tomczak, 1985; Mitchell et al., 2007b). This region receives the seasonal arrival of Bass Cascading Current (BCC), the densest seawater offshore SE Australia, along and across the continental shelf (Figure 2B; Godfrey et al., 1980). The occurrence of the BCC has resulted in extremely complex seabed geomorphology, including sediment waves, channels, canyons, gullies, and submarine landslides that are initiated from the continental shelf, and are captured by the huge Bass Canyon at the lower slope, and ultimately drain SE towards the Tasman Abyssal Plain, where water depth descends to over 4000 m (Figure 2B; Mitchell et al., 2007b). The complex seabed geomorphology reflects the action of a range of oceanographic and sedimentary processes at multiple spatiotemporal scales. Therefore, the Central Region of the Gippsland Basin provides an ideal place to investigate the remaining questions we raised previously.

This study combines new high-resolution acoustic datasets (including bathymetric multibeam, 2D and 3D seismic reflection datasets), and sediment sampling (including piston cores and grain size datasets) to comprehend the seabed geomorphologies in the Gippsland Basin. We aim to: (i) reveal the transformation process from BCC to turbidity currents; (ii) understand the hydrodynamic processes dictating seabed geomorphologies and sedimentary structures; and (iii) discuss the climate, biodiversity, and geohazard implications of the BCC and its hydrodynamic transformation.

GEOLOGICAL SETTING

The Gippsland Basin

The Gippsland Basin is one of Australia's easternmost continental margin basins. It is located in the SE corner of Australia, between the mainland of Australia and Tasmania (Figure 2A, 2B; Rahmanian et al., 1990). The Gippsland Basin belongs to a series of rift basins formed along the southern margin of the Australian plate, due to the separation of Antarctica and Australian continents during the breakup of Gondwana in the Mesozoic (Colwell et al., 1993). Since the Pleistocene, the Gippsland Basin has been detached from major river sources, allowing the development of a cool water carbonate province with minimal terrigenous input (Mitchell et al., 2007b). The margin of the Gippsland Basin is dominated by a c. 100 km wide embayment, and the SE margin of the basin is floored by c. 120 km long and 15-70 km wide, ESE-trending Bass Canyon system (Figure 2A and B). The Bass Canyon is one of the world's largest submarine canyons and constitutes the SE boundary of the Gippsland Basin (Mitchell et al., 2007b). The Bass Canyon has acted as a major conduit and key element in the source-to-sink system in the SE Australian area since the Late Cretaceous (approximately 80Ma; Hill et al., 1998). At present, it still transfers sediments, oxygen, nutrient, pollutants and organic matter from the canyon head to the Tasman Abyssal Plain at almost 4500 m water depth (Figure 2B).

Climate and oceanography

The Bass Strait is a shallow (water depth range from 40-60 m) coastal sea between mainland Australia and Tasmania, connecting the Great Australian Bight in the west and the Tasman Sea in the east (Figure 2A; Tomczak, 1985; Lavering, 1994). Compared with the seawater in the Tasman Sea, Bass Strait water is warmer and more saline (Lavering, 1994). In winter, the shallow Bass Strait imposes a limit on the penetration of thermal convection, and as a consequence, Bass Strait seawater cools rapidly and has a higher salinity than those of the surface layer in the Tasman Sea (Lavering, 1994). Therefore, when seawater leaves the Bass Strait on its eastern side, it has a prominent density contrast against the Tasman Sea water (Tomczak, 1985). As a consequence, warm, denser Bass Strait seawater can flow into and sink beneath the cooler, fresher water of the Gippsland shelf, generating the northeast flowing "Bass Cascade Current" which sinks to the 200-400 m isobaths and extends more than tens of kilometres (Figure 2B; Godfrey et al., 1980; Li et al., 2005; Mitchell et al., 2007b). Observations from the ocean bottom stations have revealed that the BCC has transported significant quantities of water and spreads along the shelf edge over a long distance (Boland, 1971). For example, distinctive temperature-salinity anomalies are found at 200-800 m depth in Tasman Sea, most likely caused by Bass Strait seawater penetration (Figure 2C; Boland, 1971).

The Bass Cascade Current (BCC) is a high-energy, seasonal (especially in winter) phenomenon. When it flows through the Bass Strait, it is further fed by the Leeuwin current (LC), Zeehan current (ZC) and the wind stress within the Bass Strait, jointly transporting Bass Strait water towards the front (Li et al., 2005; Mitchell et al., 2007b). During summer, the BCC is not active. However, strong offshore wind and tidal activities can further reinforce and transport Bass Strait water eastwards (Godfrey et al., 1980). The BCC could trigger near-bottom gravity flows (i.e. mass failure processes or turbidity currents) that transport downslope, with an average transport rate of 1.0 Sverdrups (Sv; $1Sv=10^6$ m^3/s) in the continental shelf area of Gippsland Basin (Middleton and Bye, 2007). Therefore, the BCC plays an important role in transforming sediments and other marine matter (i.e. organic carbon and marine pollutants; Mitchell et al., 2007b) in the Gippsland Basin.

In the Gippsland Basin, the central continental shelf is dominated by the Westerly wind throughout the year (see Figure 2B; especially in winter; Li et al., 2005). The eastward-flowing Westerly wind flows at 10-30 km/h with maximum gusts reaching 100 km/h. Therefore, the Westerly wind has created a moderate to high energy wave-dominated environment and a robust NE-transported Ekman Transport Flow (ETF) in a water depth of 200-350 m (Figure 1B; Mitchell et al., 2007a; O'Brien et al., 2018). The ETF can also cause upwelling events near the central shelf region, creating a high sedimentation accumulation environment (Mitchell et al., 2007a). The East Australia Current (EAC) is a western boundary current that carries warm equatorial waters and flows southward adjacent to the Australia's southeast coast (Figure 2B, 2D). It is up to 500 m deep and 100 km wide, occasionally extending far enough south to reverse the movement of water in the Gippsland Basin during summer months (Li et al., 2005). Therefore, the combination of seasonal northward flowing BCC, the southward flowing EAC, and northeast flowing ETF have jointly controlled the oceanography and sedimentation along SE Australia continental margin.

DATASET AND METHODOLOGY

The datasets available for this study include multibeam bathymetry data with a coverage area of c. 250,000 km^2, 2D and 3D seismic reflection data with a coverage area of c. 1700 km^2, with lithology control provided by six-piston core samples (Figure 2B, 3A).

Multibeam bathymetry

Multibeam bathymetry data for this study is sourced and can be downloaded from Geoscience Australia's Marine data portal (http://marine.ga.gov.au). The dataset is compiled from multiple bathymetric surveys and gridded at 50x50 m; hence, geomorphological features smaller than 50 m across cannot be differentiated. The multibeam bathymetry dataset covers the Gippsland Basin continental shelf, at around 200 m water depth, to the Tasman Sea Abyssal plain, at over 4000 m water depth (Figure 3A).

Seismic data

We adopt two types of seismic reflection data provided by Geoscience Australia (http://www.ga.gov.au/nopims): (i) 2D regional seismic section which is up to c. 90 km long, therefore providing excellent coverage from Gippsland Basin shelf region to Bass

Canyon abyssal plain (Figure 3C); and (ii) two 3D seismic reflection surveys (Elver 3D and Tuskfish 3D), which covered an area of c. 650 km^2 and 1050 km^2, respectively (Figure 2B). Both 3D seismic datasets are zero-phase processed; a downward decrease and increase in acoustic impedance are expressed as blue (negative) and red (positive) seismic reflections, respectively. The 3D seismic surveys have a dominant frequency content of 70 hertz and an average seismic velocity of 1700 m/s near the seabed sediment, which gives an approximate vertical resolution of c. 6 m for the near seabed sediments. The 3D seismic resolution is therefore sufficient to map the geometry of detailed seabed sedimentary and structural features. We further extract the dip illumination seismic attribute (see Appendix S1 for an explanation), from the 3D seismic dataset to determine the seabed geometries and geomorphology of the interpreted submarine deposits.

Piston Core and Grain Size

Comprehensive sediment sampling and piston cores collection was conducted from RV Franklin cruise in 1998 (FR11/98) (Exon et al., 2002). In this study, we adopted six-piston cores in the continental shelf and slope areas over a water depth range of 200-2500 m. The detailed core descriptions and interpretations are compiled from (Mitchell et al., 2007b), which have provided lithological and sedimentary facies constraints for the study area. In addition, we analyzed seabed grain size distribution data from 13 locations, obtained from Geoscience Australia Marine Sediment Database (https://portal.ga.gov.au). For the purpose of this current research, we analyzed the proportion of mud (<65 µm), sand (between 65 µm and 2 mm) and gravel (> 2mm) within each sampling locations.

RESULT

We divide the Gippsland Basin into Northern, Central, and Southern regions based on geographical position and seabed morphology (Figure 3A, 3B). In this study, we focus on the Central Region to conduct seabed geomorphology and sedimentary structures description, and subsequent depositional environment interpretation. The continental shelf of the Central Region extends seaward for approximately 70 km with an average dip of 0.8^o then abruptly steepens to 8.8^o in the slope (Figure 3C). The water depth ranges from 0-500 m on the shelf and from 500-2000 m on the slope (Figure 3A). Below we describe the seabed geomorphology and the major sedimentary environments from the shelf to the slope.

Seabed geomorphology of the shelf area

Observation: The Central Region is characterized by an erosional seabed (Figure 4A, 4B). On the shelf, a set of north-trending scallop-shaped scarps have been observed near the outer shelf area (Figure 4C). Seismic sections indicate the scallop-shaped scarps show a clear truncation edge and erosional base surface (termed as basal shear surface), marking the boundary that differentiates the overlying undeformed strata from the deformed sediments (Figures 5A-D). Downslope (eastward) to the scarps, a series of sediment wave fields have been observed along the middle part of the outer shelf (Figure 4B, 4C). Further downslope, the sediment waves are dissected by a set of irregular oval-shaped depressions occurring at the southwestern part of the shelf (Figure 4B, 4C). The oval-shaped depressions range from 1200-1700 m in width, 300-500 m in length, and 80-200 m in depth (Figure 4C). In the seismic section, the oval-shaped depressions are normally characterized by gently upstream-dipping, truncated, longer lee sides and steep and short stoss sides (Figure 5B). Buried oval-shaped depressions are observed beneath their seabed counterparts (Figure 5B). The internal reflections within the buried ones dip landward and aggrade in an upstream direction, and are truncated at their downstream ends and dip at an angle smaller than that of the lee side (Figure 5B).

East of the oval-shaped depressions, several sets of crescent-like bedforms that aligned in-train have been observed in the center part of the shelf (Figure 4C). The crescent-like bedforms range from 900-1200 m in length (crest to crest wavelength) and 20-60 m in wave height (Figure 4C). The crests of these crescent-like bedforms are consistently oriented approximately north-south, being confined in the axis of a channel-shaped morphology (Figure 4C). In the seismic section, a single bedform is characterized by a steep head scarp at the lee side and a gently dipping slope at the stoss side (Figure 5C, 5D). These crescent-like bedforms consist of several continuous bedforms and could stretch over a distance of 16 km (Figure 5C, 5D). Along the strike direction and further NE of the shelf, these crescent-like bedforms gradually evolve into several well-developed channels (Figure 4C).

These channels only extend to the shelf break, no clear erosions have been observed within the slope (Figure 4B, 4C). These channels vary from 2–10 km in width, and 100–325 m in depth (Figure 4B). They initially trend SSE and then sharply divert to the NE within a few kilometres distance across the shelf break, and ultimately run to the slope after passing through the shelf break (Figure 4B). A set of longitudinal lineations have been observed on the southern flank of the channels (Figure 4C). These lineations are c. 8 km long, are regularly spaced and are predominantly oriented parallel to the channel axis. In the seismic section, the longitudinal lineations show a stair-shaped cross-sectional geometry and truncations (Figure 5E).

Interpretation: The scalloped scarps developed near the outer shelf indicate a gradual broadening over time is likely caused by slope failures (i.e. Lee and Chough, 2001). The scalloped scarps are thus interpreted as headwall scarps associated with a buried landslide (Figure 5A). The oval-shaped depressions, crescent-like bedforms, and channels are developed above the landslide's basal shear surface, which suggests these bedforms were formed after the landslide deposition (Figure 5B-E). The sediment wave fields developed within the scarps is evident for the presence of downslope currents. The symmetrical cross-sectional geometries combined with upslope migration directions indicate that the crescent-like bedforms are normally formed by hydraulic jumps associated with downslope flowing currents (i.e. Taki and Parker, 2005; Fildani et al., 2013; Zhong et al., 2015). The switching of downslope flowing currents between super- and subcritical flow regimes drives the upstream migration of crescent-like bedforms (Cartigny et al., 2011). Previous studies interpret the crescent-like bedforms as cyclic steps (i.e. Fildani et al., 2006). Within a single bedform, the supercritical flow creates a hydraulic jump (Frd>1; Frd indicates Froude Number) at the base of the lee side and transfers to subcritical flow (Frd<1) at the stoss side (Figure 5C). Subsequently, the subcritical flow reaccelerates to supercritical flow again down to the lee side of the next bedform (Figure 5C).

The upslope migrating oval shaped depressions are interpreted as cyclic scours (Fildani et al., 2006; Kostic, 2011), which belong to net-erosional cyclic steps (Fildani et al., 2006). The cyclic scours are formed by the dense downslope flowing currents that excavate the seabed through the force of hydraulic jumps (Gardner et al., 2020). The buried oval-shaped depressions are interpreted as partially depositional cyclic steps, formed when sediment erosion on the lee side is less than sediment deposition on the stoss side (Slootman and Cartigny, 2020). The presence of the partially depositional cyclic steps suggests that the downslope flowing currents were active in the Central Region for an extended period of time. Mitchell et al. (2007a) suggest that these downslope flowing currents could be active since Pliocene.

Trains of the cyclic steps developed outside the channels can represent the incipient, proto stage (i.e. early incision) of future channel formation (i.e. Fildani and Normark, 2004; Fildani et al., 2013). Though the slope gradient in the central shelf is relatively low (average 0.8^{o}), the hydraulic jumps could strengthen turbulence within the parent flow, allowing the parent flow to reach the slope area (Mulder and Cochonat, 1996). The Westerly wind-induced Ekman transport flow (ETF) is potentially responsible for the channel's diversion near the shelf edge. Due to the influence of the Coriolis effect, the ETF follows a NE-NNE direction, which interacts with the sedimentary systems along the edge of the continental shelf (Mitchell et al., 2007a). Therefore, the transportation of the along shelf-edge ETF may have resulted in the downslope flowing current diversion and further redistribution of sediments. The EAC may also have contributed to the deviation of the channel axis. However, the EAC separates from the coast approximately between 30°S and 32°S, splitting into eddy-dominated southern and eastern extensions (Cetina-Heredia et al., 2014; Oke et al., 2019). The major eddies are anticlockwise, and therefore, the channel courses should be diverted to the southeast direction, which is opposite to our observation.

Within the channels, the longitudinal lineations are interpreted as sedimentary furrows similar to those observed in other submarine settings (i.e. Wynn and Stow, 2002; Puig et al., 2008). Studies of furrows show that these features were formed due to repeated turbidity currents erosion through time (e.g. Flood, 1983; Puig et al., 2008). The presence of furrows in this study suggests that the ambient downslope flowing currents may have strong and persistent energy, carrying coarse particles that erode the canyon sidewall, generating furrows (Flood, 1983). The sole appearance of furrows on the channel's southern flank suggests that the downslope flowing currents preferential arrival across the southern channel flank.

Seabed geomorphology of the slope area

Observation: Near the upper slope, gullies and landslide scarps are widely distributed on the slope between water depths 700 to 2000 m (Figure 6). The gullies extend several kilometres from the upper slope to the lower slope, terminating as the slope angle decrease and intersects with the Bass Canyon head (Figure 3A, 3B, and 6). The gullies are straight and oriented to the dip direction of the slope, characterized by linear morphology, rounded heads and narrow bodies in plain view (Figure 6). Small failures and slide scarps are evident within or around the edges of the gullies. In the seismic section, these gullies are V-shaped, having a relatively flat base reflection with clear erosive truncation along the sidewalls (Figure 7A). The gully sidewalls have a relief (incision depth) of 110-230 m, and a width of 120-280 m (Figure 7A). The landslide scarps roughly dip from NNE to SSW, with widths ranging from c. 4 km to 7km (Figure 6). In seismic sections, these scarps show a stair-shape, backward (i.e.

landward) dipping geometry (Figure 7B).

Near the lower slope, crescent-like bedforms that aligned in train and parallel to the slope dip direction have been observed within the gullies and on the inter-gully ridges (Figure 6). These bedforms are 0.5-1.3 km in wavelength and 30-70 ms in wave height, and they are characterized by steep lee sides and gentle stoss sides, similar to the cyclic steps and scours developed on the shelf (Figures 7B-D). These bedforms are best developed near the lower slope, where the slope gradient drops from 9^o-12^o (near the upper slope) to 4^o-7^o (7B-D). Further lower slope, giant landslide scarps that distribute more than 30 km horizontally are observed near the lowermost of the slope (Figure 6). In the seismic section, the scarps show clear truncations that separate the undeformed seabed (upslope) from the deformed erosional seabed (downslope) (Figures 7B-D).

Interpretation: The gullies clearly incise into the landslides, suggesting that they post-date the slope failures. The linear gullies are interpreted as the conduits for gravity flows to transport sediment to deeper waters (Micallef and Mountjoy, 2011; Lonergan et al., 2013). The V-shaped head geometry indicates the origin of the gullies is associated with downslope gravity-driven currents (i.e. debris flow and turbidity current; Farre et al., 1983; Gales et al., 2012). Successive small failures are exhibited on the gully ridges, which is indicative of a gradual widening of the gullies (Post et al., 2022). The crescent-like bedforms developed within the gullies and on the inter-gully ridges are with long and steep lee sides and short, gentle stoss sides, suggesting they are formed by the supercritical downslope flowing currents (Fildani et al., 2006). These bedforms are interpreted as cyclic steps, similar to their counterparts developed on the shelf. Therefore, the slope area is also a supercritical flow regime-dominated environment, the erosion by the overflow of supercritical currents could play a role in the initiation gully formation (i.e. Noormets et al., 2009; Gales et al., 2012).

Near the upper slope, the step-shaped pattern of the scarps suggests a retrogressive failure mechanism of the landslides (Figure 7B; Wu et al., 2021). As the landslides are located along the shelf edge, where cyclic wave loading can constantly rework seabed sediments. This process may account for a potential trigger mechanism leading to slope failure (i.e. Marshall et al., 1978; Bea et al., 1983). The construction of cyclic steps near the lower slope has led to the formation of local high topographies (Figure 7B-D). These local high topographies may act as landslide-susceptible structures that ultimately prime slope failures. Therefore, the widely distributed cyclic steps throughout the continental shelf and their continued presence near the lower slope indicate erosive and continuous downslope currents shaping and remoulding the Central Region of the Gippsland Basin.

Piston core and Grain size analysis

Observation: Facies-1 can be observed from the shelf and upper slope (Figure 4B). Facies-1 contains coarse-grained sand and is moderately to well-sorted (Figure 8A). It also comprises foraminiferal bioclasts with quartz, and decimetre-thick shell beds. Facies-1 collected from the slope area suggests this facies contains shelf-restricted bioclasts. Core observation indicates Facies-1 has a sharp top surface and an erosional base surface, and it is normally graded and rarely laminated (Figure 8A). Facies-1 is also structureless, and the lower part contains a massive sand package (mud-free). Facies-2 can be observed from the upper-lower slope (Figure 4B). Facies-2 contains sand- and silt-sized bioclasts, quartz and siliciclastic clay. Core observation indicates it is poorly sorted, matrix-supported and often organic-rich. It also has decimetre-thick bedding with gradational contacts with bioturbation observed (Figure 8B). Generally, sediment samples collected west of the landslide headwall scarps have fine-to-medium grain size, and the predominant particle diameter is between 65 µm and 2 mm (Figure 8C). In comparison, sediment sample collected within the landslide area exhibits sharp grain size variations (Figure 8C). Specifically, the sediment has an average particle diameter exceeding 2 mm and consists primarily of coarse-grained gravel.

Interpretation: The erosional base surface, coarse-grained, normally graded and internally structureless nature of Facies-1 is a typical indicator of Bouma Ta-typed turbidites (Bouma, 1962). The abundance of shelf-restricted bioclasts observed from the slope suggests these turbidites originated from the shelf. Therefore, we interpret Facies-1 as turbidity currents sourced from the continental shelf. The poorly sorted and organic-rich nature of Facies-2 suggests it is deposited under a low energy condition. We interpret Facies-2 represents a deep marine hemipelagic environment (Mitchell et al., 2007b). Grain size variation between the undeformed seabed and the landslide area suggests a shift in the current regime and an increase in current energy. This contrast may be attributed to the transition from along shelf-edge transported lower energy BCC to downslope transported higher energy turbidity current (Postma and Cartigny, 2014). Thus, coarse-grained sediment can be resuspended and transported to the landslide area by turbidity currents.

DISCUSSION

Supercritical turbidity current: the dominant sedimentary process in central Gippsland Basin

The core observation and grain size analyses have already shown that the downslope flowing currents that are prevalent in the Central Region are turbidity currents. Due to the presence of cyclic steps and scours, it is most likely that the turbidity currents belong to supercritical turbidity currents (i.e. Fildani et al., 2006; Zhong et al., 2015). Core observation is consistent with this interpretation, as recent publications suggest that Ta-typed turbidites are formed by hydraulic jump-related rapid sedimentation, often associated with high-energy supercritical turbidity currents (Figure 8A; i.e. Postma and Cartigny, 2014). Fully developed supercritical bedforms (cyclic steps and scours) are particularly common throughout the shelf and slope areas, which indicate a continuing role of supercritical turbidity currents in sculpting the seabed in the Central Gippsland Basin (i.e. Kostic, 2011; Zhong et al., 2015).

Though the slope gradient on the shelf is c. 0.8°, hydraulic jumps could greatly enhance turbulence within turbidity currents (Mulder and Cochonat, 1996), promoting the erosional process and maintaining the steep gradient of the lee side (Fildani et al., 2006). The steep gradient of the lee side can sustain the hydraulic jump, and facilitate long runout distances of turbidity currents (Fildani et al., 2006). Therefore, the turbidity currents could transport across the shelf over a long distance and reach the slope area. On the slope, cyclic steps preferentially form near the lower slope area, where the slope gradient is relatively small (Figure 7B-D). This observation indicates that a gentle slope gradient (thus a lower densimetric Froude number) can facilitate the formation of hydraulic jumps, which is consistent with the published works (i.e. Fildani et al., 2006; Zhong et al., 2015). We suggest that lower slope gradients could limit the ability of the streamwise pull of the turbidity currents to decelerate and form hydraulic jumps (Kostic, 2011).

An overlooked process: the transformation of dense cascading water into supercritical turbidity current

Turbidity currents are generally caused by slope failures and their associated debris flows, or hyperpycnal flows from onshore fluvial input (Talling et al., 2013; Paull et al., 2018). However, the Central Region has been completely disconnected from onshore drainage systems since Pliocene (Mitchell et al., 2007b), and no modern submarine landslides (only buried landslides are observed on the shelf) are observed in the central shelf. Therefore, the initiation of the turbidity currents cannot be caused by either slope failures or hyperpycnal flows. Previous studies indicated that the BCC could increase sedimentation rates and directly trigger turbidity currents across the Gippsland Basin shelf area (Mitchell et al., 2007b). Below we discuss how the BCC could trigger turbidity currents in the Gippsland Basin.

While the BCC flows along the shelf edge of the Gippsland Basin, it also spreads around the shelf break (Figure 9A). In fact, the saline bottom water of BCC will be driven eastward during winter and flows off the edge of the continental shelf and down the continental slope and beneath the EAC (Godfrey et al., 1980). The transportation of BCC could generate bottom nepheloid layers that contain significant amounts of suspended sediments (Figure 9A, 9B; Puig, 2017). The prevalence of headwall scarps developed near the outer shelf has provided a rugose seabed topography that catches the nepheloid layers and forces them to sink (Figure 9C). The headwall scarps also offer the initial perturbations for the suspended sediments, increasing their velocity and promoting the spontaneous hydraulic jumps and forming supercritical turbidity currents (Figure 9B, 9C; i.e. Cartigny et al., 2011; Lang et al., 2017). Other oscillatory oceanographic processes, including Westerly winds generated strong wave actions, storms, tide-generated currents and EAC realted eddies, may coincide with the BCC and jointly resuspend large amounts of seabed sediments and generate downslope flows that contribute to turbidity current initiation (Figure 9D; Cacchione et al., 2002; Micallef and Mountjoy, 2011; Talling et al., 2013).

Similar examples of strong DSWC events transporting sediments over long distances and initiated turbidity currents from the shelf region have been documented in offshore Antarctica (Noormets et al., 2009), on the Norwegian margins (Laberg and Vorren, 1995), and in the Hikurangi subduction margin, New Zealand (Micallef and Mountjoy, 2011). Our study reveals for the first time that the DSWC could transform into supercritical turbidity currents, and this current transformation has played a key role in the long-distance transportation of shelf water, which accounts for sediment, organic carbon, marine pollutants and plastic litter transfer from shallow marine (i.e. shelf edge) to deep marine (i.e. lower slope).

The evolution of seabed geomorphology

The supercritical turbidity currents are an effective seabed sculpting tool and hugely influenced the modern seabed geomorphology and sedimentation in the Gippsland Basin. On the shelf, the spatial relationship among cyclic scours, cyclic steps, and channels represents a channel evolution sequence. (Figure 10A, 10B). The cyclic scours and cyclic step trains represent morphodynamic signals of the early establishment of channels traversed by supercritical turbidity currents (initial erosional phase; Fildani et al., 2013). The incipient channels could develop into matured channels and further evolve to canyons under the continuous erosion associated with supercritical turbidity currents (Figure 10C; Mitchell et al., 2007b). On the slope, the supercritical turbidity currents have resulted in considerable seabed erosion, generating widespread gullies that represent a relatively immature drainage system (Figure 10B; Santangelo et al., 2013). With the continuous downslope transportation of the supercritical turbidity currents and other gravity flows (i.e. submarine landslide), the gullies will act as preferential conduits for large-scale sediment transfer and may evolve into canyons (Figure 10C; Santangelo et al., 2013).

Implications

For biodiversity

The intense turbidity currents developed on the continental shelf could deliver nutrients and provide an intermediate disturbance regime to submarine biological communities (i.e. cold-water corals and other marine species), which significantly enhances biodiversity (Danovaro et al., 2009; Harris, 2014). As the BCC sinks, low salinity nutrient-rich waters could upwell off the shelf edge and supports local biodiversity (James and Bone, 2010). In addition, the gullies developed along the shelf edge and continental slope could provide an ideal host to biosystems, as their rugose floor and steep sidewalls have a greater surface area than the surrounding seabed, thus creating a suitable living condition for marine life (Moors-Murphy, 2014; Post et al., 2022). The diversity of the marine ecosystems (i.e. cold-water corals and marine lives) and their sensitivity to the sedimentary processes variation and environmental heterogeneity (Vetter et al., 2010; Hebbeln et al., 2016; Post et al., 2022). Additionally, these flows could contribute to global carbon flux and aid the transportation of pollutants to the deep sea (Zhong and Peng, 2021).

For natural hazard mitigation

In 2022, the Australian Government announced new wind farm construction plans on the Victorian Coast in the Gippsland Basin (the same area as this study; see from Victorian State Government website). However, our results indicate supercritical turbidity currents have dominated the shelf area of the Gippsland Basin. The emplacement of supercritical turbidity currents can directly damage submarine installations (i.e., breakup seabed telecommunication cables; Carter et al., 2014) and damage submarine pipelines that may cause potential hydrocarbon leakage hazards (Porcile et al., 2020). Therefore, we suggest that future marine spatial planning and offshore constructions should consider a reasonable band of the buffer zone (e.g. 10-20 km wide) landward to the landslide headwall scarps located in the central shelf (i.e. Figure 10C). We also indicate that new geological and geophysical datasets (including sedimentary cores, grabbing or dredging samples, additional 3D seismic reflection data, crewed submersible dives, and Autonomous Underwater Vehicles) need to assess modern seabed conditions (oceanographic and geomorphology), to provide better suggestions for future assessments.

The link between climate change and seabed geomorphology evolution

As the climate warms, the temperature of the oceans will inevitably increase (Pittock, 2017). The seasonal hydrodynamic Bass Cascade Current is sensitive to seawater temperature variation that can significantly influence the velocity, pathway, and strength of such a current (Herrmann et al., 2008; Puig, 2017). Extreme climate perturbations can alter the oceanographic condition and form extremely dense water over human time scales (i.e. a centennial or longer scale; Micallef and Mountjoy, 2011). The formation of the dense shelf water can transport great distances along and cascade down to the continental shelf and slope, posing significant impacts on the seabed geomorphology evolution. The impact of climate change on the intensity of the BCC also can be related to its countercurrent - the EAC, which is remarkably sensitive to both short and long-term climate variations. As the BCC and EAC flow in opposite directions on the shelf, a weaker EAC may enhance the BCC, while a strong EAC may flow far south and compensate for the influences of the BCC (Oke et al., 2019).

In addition, climate change can alter ocean heat supply which is projected to cause variations in seawater temperature or salinity (Canals et al., 2009; Gales et al., 2021). The variation of seawater temperature and/or salinity could significantly impact the pathway and strength of the dense water cascading currents and, thus, the seabed geomorphology and sedimentation process. In Gippsland Basin, we suggest additional higher resolution datasets (i.e. 3D seismic reflection data) and sedimentological information (scientific drillings) are required to better constrain the links between oceanographic processes and seabed geomorphology evolution. We also acknowledge that future numerical modelling-based studies in other continental margins, which are dominated by dense cascading water, are needed to validate our hypothesis that climate change could induce variations in near-seabed sedimentary processes via controlling the cascading water.

CONCLUSION

This study reveals the evolution of seabed geomorphology and sedimentary processes through time under the influence of dynamic climate and oceanographic processes in the central Gippsland Basin. The Bass Cascade Current and Westerly winds have resulted in a dynamic sedimentary process that has left a number of geomorphological features. We envisage that the transformation from the Bass Cascade Current into supercritical turbidity currents has a major role in the long distance of nearshore water cross-shelf transportation and also contributes significantly to seabed geomorphological evolution. The detailed morphological study of the seabed allows us to identify specific regions of hazard, which has a significant implication for hazard mitigation and can provide key geological information for submarine infrastructure construction projects. We suggest that due to the warming of the atmosphere, future extreme weather can predominately influence the seabed geomorphology, sedimentation process and occurrence of geohazards in the Gippsland Basin and on different continental margins worldwide.

ACKNOWLEDGMENTS

This research was supported by the Fundamental Research Funds for the Central Universities, China. The first author thanks the Shanghai Sailing Program (under Grant No. 22YF1450100) and the State Key Laboratory of Marine Geology (under Grant No. MGZ202303) for their financial support. We thank Geoscience Australia for providing seismic reflection, multibeam bathymetry, and grain size data for the Gippsland Basin and Bass Canyon. Seismic reflection, multibeam bathymetry and grain size data are available from the Geoscience Australia Data Portal: https://portal.ga.gov.au/persona/marine. We thank Dr Xingxing Wang, Dr Wei Li, and Dr Yongpeng Qin for their helpful discussions during the preparation of this paper.

FIGURE CAPTIONS

Figure 1. (A) Occurrence previously documented dense shelf water cascade (DSWC) around the world. Numbers in each area of the Figure refer to the location: (1) Eastern Chukchi Sea shelf, (2) Beaufort Sea shelf, (3) Foxe Basin, (4) SW Greenland margin, (5) Northern gulf of California, (6) North American southeastern shelf, (7) Great Bahama Bank, (8) Rockall Bank, (9) Celtic Sea shelf, (10) Banc d'Arguin, (11) Skagerrak, (12) Adriatic Sea shelf, (13) Southern Mediterranean Sea shelf, (14) Aegean Sea shelf, (15) Western shelf of Novaya Zemlya, (16) shelf of Nansen Basin, (17) North-eastern Severnaya Zemlya shelf, (18) Peter the Great Bay, (19) Northern sea of Okhotsk, (20) NW Australia inner shelf, (21) Shark Bay, (22) Great Australian Bight, (23) Jervis Bay, (24) Bass Strait, (25) Spencer Gulf, (26) Ross Sea shelf, and (27) Weddell Sea shelf. The location of the DSWC atlas is adopted from Ivanov et al. (2004) and Mahjabin et al. (2020). (B) Schematics of the DSWC mechanism showing the formation of intermediate nepheloid layers on the shelf and the downslope turbidity currents. Adapted from Fohrmann et al. (1998).

Figure 2. (A) The regional map of Australia, showing the location of the study area (indicated in a red polygon) and the oceanographic setting. The trajectories of the main oceanic currents are represented by white, blue, and yellow dashed lines. LC, Leeuwin Current; SAC, South Australian Current; ZC, Zeehan Current; BCC, Bass Cascade Current; EAC, East Australian Current. (B) Zoom in view of the study area, showing the region of the Gippsland Basin and the Bass Canyon. Note the north arrow (white) and the yellow box denote the location of the 3D seismic data. The transportation pathway of the BCC is adopted from Tomczak (1985). The transportation pathway of the EAC is adopted from Lavering (1994) and Ridgway and Hill (2009). (C) Temperature profile of the Bass Strait showing the downward high-temperature anomalies within the continental shelf and slope. The temperature data is from the Upper Ocean Thermal Program (available athttps://odv.awi.de/data/ocean). See Figure 2A for location. (D) Temperature profile (potential temperature) in offshore eastern Australia, showing the

depth of the East Australian Current (EAC). The temperature data is from the WOCE (World Ocean Current Experiment) Hydrographic Program (available at https://odv.awi.de/data/ocean). See Figure 2A for locations.

Figure 3. (A) 3D seabed multibeam bathymetric map of the offshore Gippsland Basin and Bass Canyon system, showing the main geomorphologic features. (B) Sketch of Figure 3A, showing the key depositional elements, canyons and distinguished regional domains. (C) Shelf-to-slope seismic profile showing the Central shelf and slope regions. See Figure 3B for location.

Figure 4. (A) Seabed structure map generated from the 3D seismic data, showing the seabed morphology in the Central Region. (B) Dip illumination attribute map calculated from the 3D seismic data, showing the detailed sedimentary structures of the Central Region. Note the yellow dots indicate the piston core location. (C) Zoomed-in view of the continental shelf in the Central Region, emphasizing the sediment waves, cyclic scours, cyclic steps and channels. See Figure 4B for location.

Figure 5. (A) Seismic dip section cut through the headwall scarp of the landslide. (B) Seismic dip section cutting through cyclic scours. (C) Seismic dip section cutting through cyclic steps. The inserted schematic map shows a series of idealized asymmetrical cyclic steps and hypothetical densiometric Froude number (Fr) variability. The schematic map was modified by Cartigny et al. (2011). (D) Seismic dip section cutting through cyclic steps. (E) Seismic section cutting through the channels; note the stair-shaped erosional characteristics of furrows developed on the channel sidewalls. See Figure 4C for locations.

Figure 6. Zoomed-in view of the continental slope in the Central Region, emphasizing the landslides and gullies. See Figure 4B for location.

Figure 7. (A) Seismic section illustrating gullies' cross-sectional geometries. (B) Seismic

dip section cutting along the gully ridge. (C) Seismic dip section cutting along the gully ridge. (D) Seismic dip section cutting within the gully and along its thalweg. See Figure 6 for locations.

Figure 8. (A) Core sketch generated based on piston core report, showing the cross-section of the Facies-1. Figure 8A is modified from Postma and Cartigny (2014). (B) Core sketch showing the cross-section of Facies-2. (C) Grain size distribution in the Central area of the Gippsland Basin. The blue arrow indicates the transport direction of the BCC.

Figure 9. (A) The 3D view of the Central Region, showing the seabed morphological structures and major current pathways. (B) Schematic 2D plain view of the Central shelf, illustrating the location of headwall scarps, the pathway of the BCC and its associated supercritical turbidity currents. See Figure 9A for location. (C) Schematic cross-section showing the transformation from BCC to supercritical turbidity currents. See Figure 9B for location. (D) Schematic cross-section depicting the combined influence of the Westerly Wind, internal waves, and tide-induced sediment resuspension and turbidity current initiation. See Figure 9A for location.

Figure 10. Schematic of seabed geomorphology evolution processes in the Central Region of the Gippsland Basin. (A) Shelf: the transformation of the Bass Cascading Current (BCC) into turbidity currents; Slope: the generation of scarps caused by wave activities near the upper slope. (B) Shelf: The formation of the sedimentary structures caused turbidity currents; Slope: The initiation of gullies and the formation of the landslides on the upper slope. (C) Shelf: The evolution from cyclic steps into channels and canyons; Slope: landslide initiation near the lower slope.

REFERENCE

Bouma, A. H. P. H. K. F. P. S., 1962, Sedimentology of some Flysch deposits : a graphic approach to facies interpretation, Amsterdam Elsevier, 168 p.:

Boland, F., 1971, Temperature-salinity anomalies at depths between 200m and 800m in the Tasman sea: Marine and Freshwater Research, v. 22, no. 2, p. 55-62.

Marshall, N., Stanley, D., and Kelling, G., 1978, Large storm-induced sediment slump reopens an unknown Scripps submarine canyon tributary: Sedimentation in submarine canyons, fans, and trenches: Stroudsburg, Pennsylvania, Hutchinson and Ross, p. 73-84.

Godfrey, J., Jones, I., Maxwell, G., and Scott, B., 1980, On the winter cascade from Bass Strait into the Tasman Sea: Marine and Freshwater Research, v. 31, no. 3, p. 275-286.

Bea, R. G., Wright, S. G., Sircar, P., and Niedoroda, A. W., 1983, Wave-induced slides in south pass block 70, Mississippi Delta: Journal of Geotechnical Engineering, v. 109, no. 4, p. 619-644.

Farre, J. A., McGregor, B. A., Ryan, W. B., and Robb, J. M., 1983, Breaching the shelfbreak: passage from youthful to mature phase in submarine canyon evolution.

Flood, R. D., 1983, Classification of sedimentary furrows and a model for furrow initiation and evolution: Geological Society of America Bulletin, v. 94, no. 5, p. 630-639.

Tomczak, 1985, The Bass Strait water cascade during winter 1981: Continental Shelf Research, v. 4, no. 3, p. 255-278.

Rahmanian, V., Moore, P., Mudge, W., and Spring, D., 1990, Sequence stratigraphy and the habitat of hydrocarbons, Gippsland Basin, Australia: Geological Society, London, Special Publications, v. 50, no. 1, p. 525-544.

Colwell, J. B., Constantine, A. E., and Willcox, J. B., 1993, Regional structure of the Gippsland Basin: interpretation and mapping of a deep seismic data set, Australian Geological Survey Organisation.

Lavering, I. H., 1994, Marine environments of Southeast Australia (Gippsland Shelf and Bass Strait) and the impact of offshore petroleum exploration and production activity: Marine georesources & geotechnology, v. 12, no. 3, p. 201-226.

Laberg, J., and Vorren, T., 1995, Late Weichselian submarine debris flow deposits on the Bear Island Trough mouth fan: Marine Geology, v. 127, no. 1-4, p. 45-72.

Mulder, T., and Cochonat, P., 1996, Classification of offshore mass movements: Journal of Sedimentary research, v. 66, no. 1, p. 43-57.

Fohrmann, H., Backhaus, J. O., Blaume, F., and Rumohr, J., 1998, Sediments in bottom-arrested gravity plumes: Numerical case studies: Journal of Physical Oceanography, v. 28, no. 11, p. 2250-2274.

Hill, P., Exon, N., Keene, J., and Smith, S., 1998, The continental margin off east Tasmania and Gippsland: structure and development using new multibeam sonar data: Exploration Geophysics, v. 29, no. 4, p. 410-419.

Lee, S., and Chough, S., 2001, High‐resolution (2–7 kHz) acoustic and geometric characters of submarine creep deposits in the South Korea Plateau, East Sea: Sedimentology, v. 48, no. 3, p. 629-644.

Cacchione, D., Pratson, L. F., and Ogston, A., 2002, The shaping of continental slopes by internal tides: Science, v. 296, no. 5568, p. 724-727.

Exon, N., Hill, P., Partridge, A., Chaproniere, G., and Keene, J., 2002, Cretaceous volcanogenic and Miocene calcareous strata dredged from the deepwater Gippsland Basin on RV Franklin Research Cruise FR11/98: Geoscience Australia Record, v. 7.

Wynn, R. B., and Stow, D. A., 2002, Recognition and interpretation of deep-water sediment waves-implications for palaeoceanography, hydrocarbon exploration and flow process interpretation (Introduction to special issue): Marine Geology, v. 192, no. 1-3, p. 1-3.

Fildani, A., and Normark, W. R., 2004, Late Quaternary evolution of channel and lobe complexes of Monterey Fan: Marine Geology, v. 206, no. 1-4, p. 199-223.

Ivanov, V., Shapiro, G., Huthnance, J., Aleynik, D., and Golovin, P., 2004, Cascades of dense water around the world ocean: Progress in oceanography, v. 60, no. 1, p. 47-98.

Li, F., Dyt, C., Griffiths, C., Jenkins, C., Rutherford, M., and Chittleborough, J., 2005, Seabed sediment transport and offshore pipeline risks in the Australian southeast: The APPEA Journal, v. 45, no. 1, p. 523-534.

Taki, K., and Parker, G., 2005, Transportational cyclic steps created by flow over an erodible bed. Part 1. Experiments: Journal of Hydraulic Research, v. 43, no. 5, p. 488-501.

Canals, M., Puig, P., de Madron, X. D., Heussner, S., Palanques, A., and Fabres, J., 2006, Flushing submarine canyons: Nature, v. 444, no. 7117, p. 354-357.

Fildani, A., Normark, W. R., Kostic, S., and Parker, G., 2006, Channel formation by flow stripping: Large‐scale scour features along the Monterey East Channel and their relation to sediment waves: Sedimentology, v. 53, no. 6, p. 1265-1287.

Palanques, A., de Madron, X. D., Puig, P., Fabres, J., Guillén, J., Calafat, A., Canals, M., Heussner, S., and Bonnin, J., 2006, Suspended sediment fluxes and transport processes in the Gulf of Lions submarine canyons. The role of storms and dense water cascading: Marine Geology, v. 234, no. 1-4, p. 43-61.

Middleton, J. F., and Bye, J. A., 2007, A review of the shelf-slope circulation along Australia's southern shelves: Cape Leeuwin to Portland: Progress in Oceanography, v. 75, no. 1, p. 1-41.

Mitchell, J., Holdgate, G., and Wallace, M., 2007a, Pliocene–Pleistocene history of the Gippsland Basin outer shelf and canyon heads, southeast Australia: Australian Journal of Earth Sciences, v. 54, no. 1, p. 49-64.

Mitchell, J., Holdgate, G., Wallace, M., and Gallagher, S., 2007b, Marine geology of the Quaternary Bass Canyon system, southeast Australia: a cool-water carbonate system: Marine geology, v. 237, no. 1-2, p. 71-96.

Herrmann, M., Estournel, C., Déqué, M., Marsaleix, P., Sevault, F., and Somot, S., 2008, Dense water formation in the Gulf of Lions shelf: Impact of atmospheric interannual variability and climate change: Continental Shelf Research, v. 28, no. 15, p. 2092-2112.

Puig, P., Palanques, A., Orange, D., Lastras, G., and Canals, M., 2008, Dense shelf water cascades and sedimentary furrow formation in the Cap de Creus Canyon, northwestern Mediterranean Sea: Continental Shelf Research, v. 28, no. 15, p. 2017-2030.

Canals, M., Danovaro, R., Heussner, S., Lykousis, V., Puig, P., Trincardi, F., Calafat, A. M., de Madron, X. D., Palanques, A., and Sanchez-Vidal, A., 2009, Cascades in Mediterranean submarine grand canyons: Oceanography, v. 22, no. 1, p. 26-43.

Danovaro, R., Canals, M., Gambi, C., Heussner, S., Lampadariou, N., and Vanreusel, A., 2009, Exploring benthic biodiversity patterns and hotspots on European margin slopes: Oceanography, v. 22, no. 1, p. 16-25.

Noormets, R., Dowdeswell, J., Larter, R. D., Cofaigh, C. Ó., and Evans, J., 2009, Morphology of the upper continental slope in the Bellingshausen and Amundsen Seas–Implications for sedimentary processes at the shelf edge of West Antarctica: Marine Geology, v. 258, no. 1-4, p. 100-114.

Ridgway, K., and Hill, K., 2009, The East Australian Current.

James, N. P., and Bone, Y., 2010, Neritic carbonate sediments in a temperate realm: southern Australia, Springer Science & Business Media.

Vetter, E. W., Smith, C. R., and De Leo, F. C., 2010, Hawaiian hotspots: enhanced megafaunal abundance and diversity in submarine canyons on the oceanic islands of Hawaii: Marine Ecology, v. 31, no. 1, p. 183-199.

Cartigny, M. J., Postma, G., Van den Berg, J. H., and Mastbergen, D. R., 2011, A comparative study of sediment waves and cyclic steps based on geometries, internal structures and numerical modeling: Marine Geology, v. 280, no. 1-4, p. 40-56.

Kostic, S., 2011, Modeling of submarine cyclic steps: Controls on their formation, migration, and architecture: Geosphere, v. 7, no. 2, p. 294-304.

Micallef, A., and Mountjoy, J. J., 2011, A topographic signature of a hydrodynamic origin for submarine gullies: Geology, v. 39, no. 2, p. 115-118.

Gales, J., Larter, R., Mitchell, N., Hillenbrand, C. D., Østerhus, S., and Shoosmith, D., 2012, Southern Weddell Sea shelf edge geomorphology: Implications for gully formation by the overflow of high‐salinity water: Journal of Geophysical Research: Earth Surface, v. 117, no. F4.

Fildani, A., Hubbard, S. M., Covault, J. A., Maier, K. L., Romans, B. W., Traer, M., and Rowland, J. C., 2013, Erosion at inception of deep-sea channels: Marine and Petroleum Geology, v. 41, p. 48-61.

Lonergan, L., Jamin, N. H., Jackson, C. A.-L., and Johnson, H. D., 2013, U-shaped slope gully systems and sediment waves on the passive margin of Gabon (West Africa): Marine Geology, v. 337, p. 80-97.

Santangelo, M., Gioia, D., Cardinali, M., Guzzetti, F., and Schiattarella, M., 2013, Interplay between mass movement and fluvial network organization: An example from southern Apennines, Italy: Geomorphology, v. 188, p. 54-67.

Talling, P. J., Paull, C. K., and Piper, D. J., 2013, How are subaqueous sediment density flows triggered, what is their internal structure and how does it evolve? Direct observations from monitoring of active flows: Earth-Science Reviews, v. 125, p. 244-287.

Carter, L., Gavey, R., Talling, P. J., and Liu, J. T., 2014, Insights into submarine geohazards from breaks in subsea telecommunication cables: Oceanography, v. 27, no. 2, p. 58-67.

Cetina‐Heredia, P., Roughan, M., Van Sebille, E., and Coleman, M., 2014, Long‐term trends in the East Australian Current separation latitude and eddy driven transport: Journal of Geophysical Research: Oceans, v. 119, no. 7, p. 4351-4366.

Harris, P. T., 2014, Shelf and deep-sea sedimentary environments and physical benthic disturbance regimes: a review and synthesis: Marine Geology, v. 353, p. 169-184.

Moors-Murphy, H. B., 2014, Submarine canyons as important habitat for cetaceans, with special reference to the Gully: a review: Deep Sea Research Part II: Topical Studies in Oceanography, v. 104, p. 6-19.

Postma, G., and Cartigny, M. J., 2014, Supercritical and subcritical turbidity currents and their deposits—A synthesis: Geology, v. 42, no. 11, p. 987-990.

Zhong, G., Cartigny, M. J., Kuang, Z., and Wang, L., 2015, Cyclic steps along the South Taiwan Shoal and West Penghu submarine canyons on the northeastern continental slope of the South China Sea: Bulletin, v. 127, no. 5-6, p. 804-824.

Hebbeln, D., Van Rooij, D., and Wienberg, C., 2016, Good neighbours shaped by vigorous currents: Cold-water coral mounds and contourites in the North Atlantic: Marine Geology, v. 378, p. 171-185.

Lang, J., Brandes, C., and Winsemann, J., 2017, Erosion and deposition by supercritical density flows during channel avulsion and backfilling: Field examples from coarse-grained deepwater channel-levée complexes (Sandino Forearc Basin, southern Central America): Sedimentary Geology, v. 349, p. 79-102.

Pittock, A. B., 2017, Climate change: turning up the heat, Routledge.

Puig, P., 2017, Dense shelf water cascading and associated bedforms, Atlas of bedforms in the western mediterranean, Springer, p. 35-40.

O'Brien, P., Mitchell, C., Nguyen, D., and Langford, R., 2018, Mass Transport Complexes on a Cenozoic paleo-shelf edge, Gippsland basin, southeastern Australia: Marine and Petroleum Geology, v. 98, p. 783-801.

Paull, C. K., Talling, P. J., Maier, K. L., Parsons, D., Xu, J., Caress, D. W., Gwiazda, R., Lundsten, E. M., Anderson, K., and Barry, J. P., 2018, Powerful turbidity currents driven by dense basal layers: Nature communications, v. 9, no. 1, p. 1-9.

Oke, P. R., Roughan, M., Cetina-Heredia, P., Pilo, G. S., Ridgway, K. R., Rykova, T., Archer, M. R., Coleman, R. C., Kerry, C. G., and Rocha, C., 2019, Revisiting the circulation of the East Australian Current: Its path, separation, and eddy field: Progress in Oceanography, v. 176, p. 102139.

Gardner, J. V., Peakall, J., Armstrong, A. A., and Calder, B. R., 2020, The Geomorphology of Submarine Channel Systems of the Northern Line Islands Ridge, Central Equatorial Pacific Ocean: Frontiers in Earth Science, v. 8, p. 87.

Mahjabin, T., Pattiaratchi, C., and Hetzel, Y., 2020, Occurrence and seasonal variability of Dense Shelf Water Cascades along Australian continental shelves: Scientific reports, v. 10, no. 1, p. 1-13.

Morrison, A., Hogg, A. M., England, M. H., and Spence, P., 2020, Warm Circumpolar Deep Water transport toward Antarctica driven by local dense water export in canyons: Science advances, v. 6, no. 18, p. eaav2516.

Porcile, G., Bolla Pittaluga, M., Frascati, A., and Sequeiros, O. E., 2020, Typhoon-induced megarips as triggers of turbidity currents offshore tropical river deltas: Communications Earth & Environment, v. 1, no. 1, p. 1-13.

Slootman, A., and Cartigny, M. J., 2020, Cyclic steps: Review and aggradation-based classification: Earth-Science Reviews, v. 201, p. 102949.

Gales, J., Rebesco, M., De Santis, L., Bergamasco, A., Colleoni, F., Kim, S., Accettella, D., Kovacevic, V., Liu, Y., and Olivo, E., 2021, Role of dense shelf water in the development of Antarctic submarine canyon morphology: Geomorphology, v. 372, p. 107453.

Wu, N., Nugraha, H. D., Zhong, F. G., and Steventon, M., 2021, The role of mass-transport complexes (MTCs) in the initiation and evolution of submarine canyons.

Zhong, G., and Peng, X., 2021, Transport and accumulation of plastic litter in submarine canyons—The role of gravity flows: Geology, v. 49, no. 5, p. 581-586.

Post, A. L., Przeslawski, R., Nanson, R., Siwabessy, J., Smith, D., Kirkendale, L. A., and Wilson, N. G., 2022, Modern dynamics, morphology and habitats of slope-confined canyons on the northwest Australian margin: Marine Geology, v. 443, p. 106694.

Figure 1

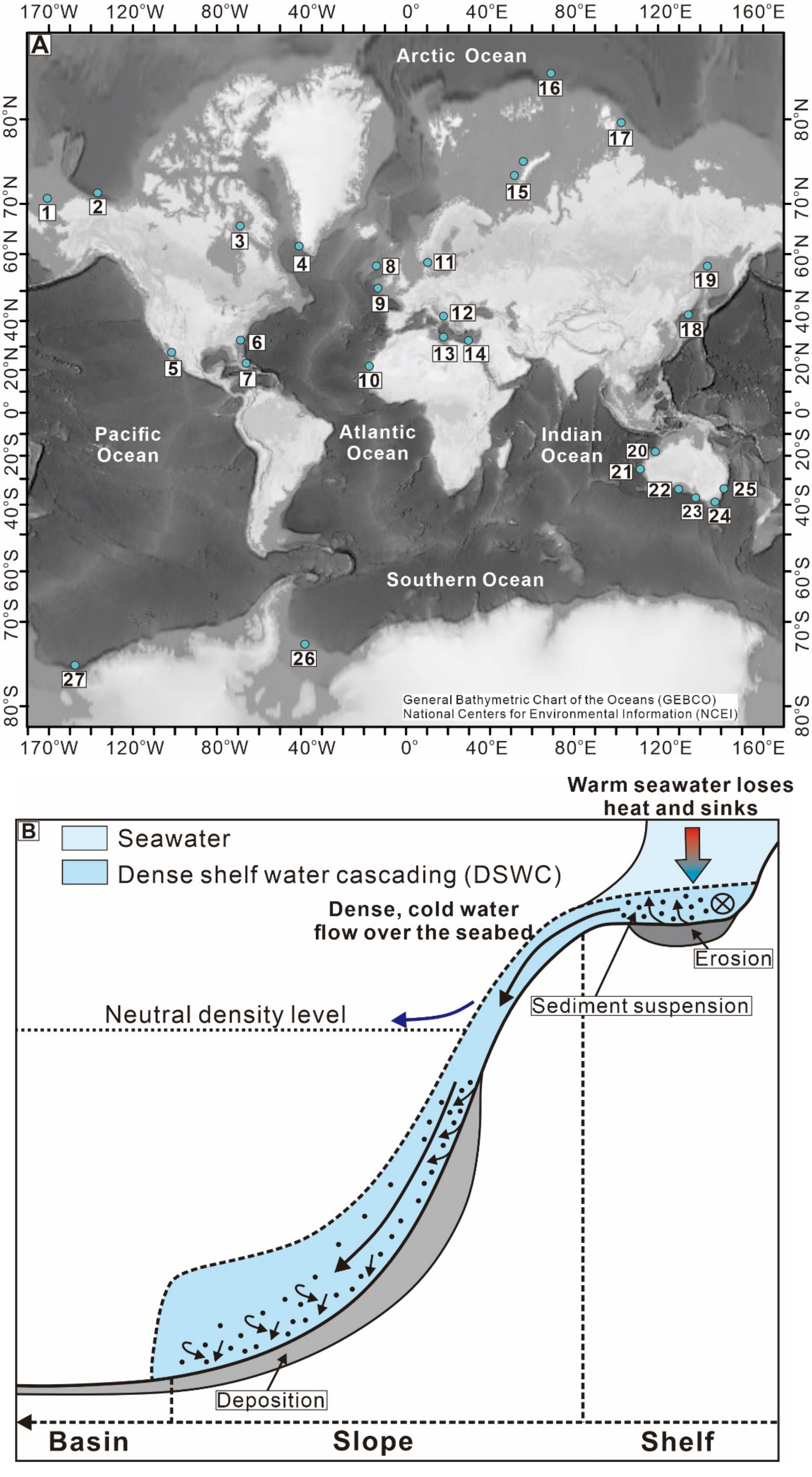

A
Arctic Ocean
Pacific Ocean
Atlantic Ocean
Indian Ocean
Southern Ocean
General Bathymetric Chart of the Oceans (GEBCO)
National Centers for Environmental Information (NCEI)
B
Seawater
Dense shelf water cascading (DSWC)
Warm seawater loses heat and sinks
Dense, cold water flow over the seabed
Erosion
Sediment suspension
Neutral density level
Deposition
Basin
Slope
Shelf

Figure 2

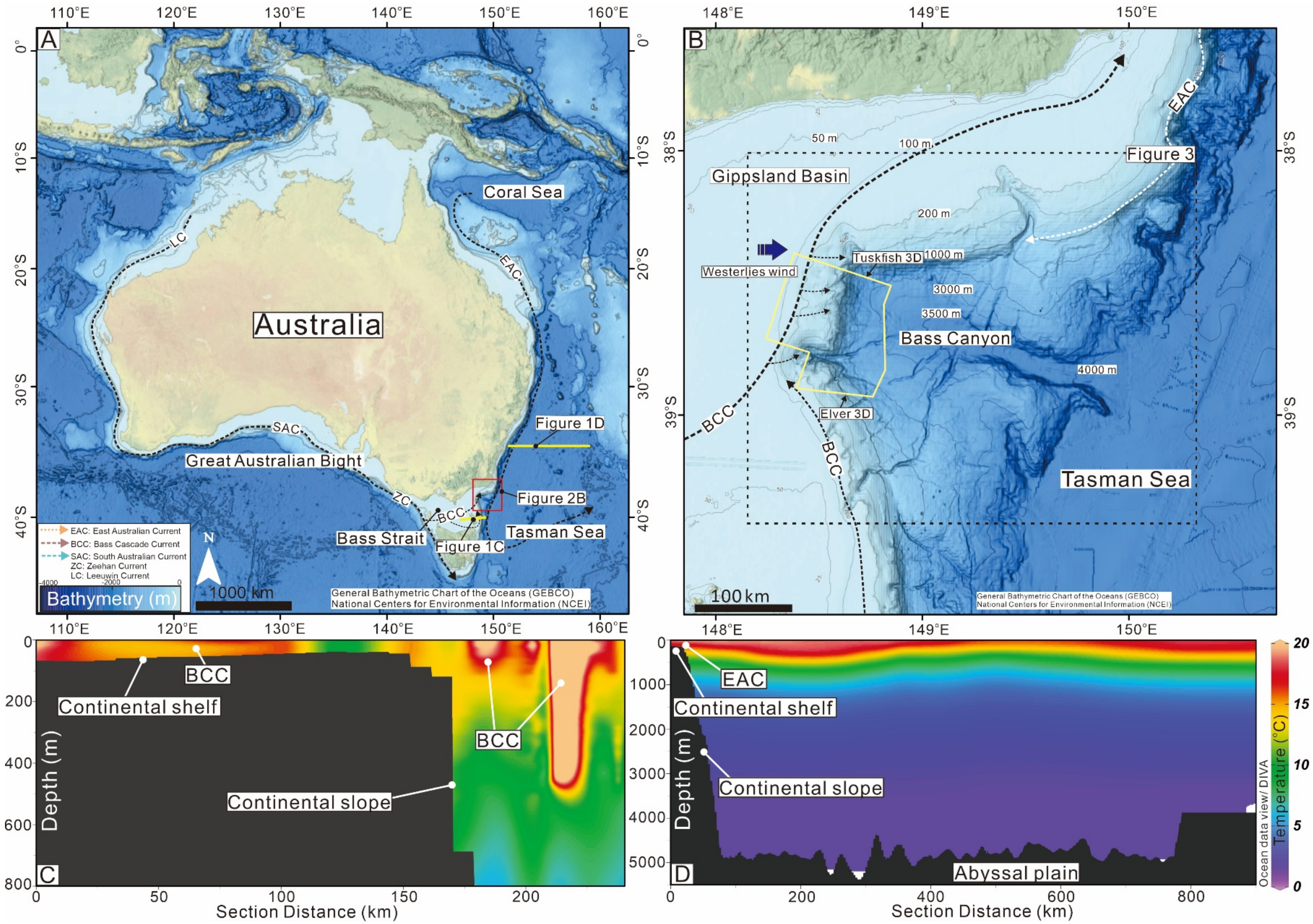

A
B
C
D
Australia
Coral Sea
Great Australian Bight
Bass Strait
Tasman Sea
Figure 1D
Figure 2B
Figure 1C
LC
EAC
SAC
ZC
BCC
EAC: East Australian Current
BCC: Bass Cascade Current
SAC: South Australian Current
ZC: Zeehan Current
LC: Leeuwin Current
Bathymetry (m)
1000 km
General Bathymetric Chart of the Oceans (GEBCO)
National Centers for Environmental Information (NCEI)
Gippsland Basin
Figure 3
Westerlies wind
Tuskfish 3D
Elver 3D
Bass Canyon
50 m
100 m
200 m
1000 m
3000 m
3500 m
4000 m
100 km
Continental shelf
Continental slope
Abyssal plain
Depth (m)
Section Distance (km)
Temperature (°C)
Ocean data view/ DIVA

Figure 3

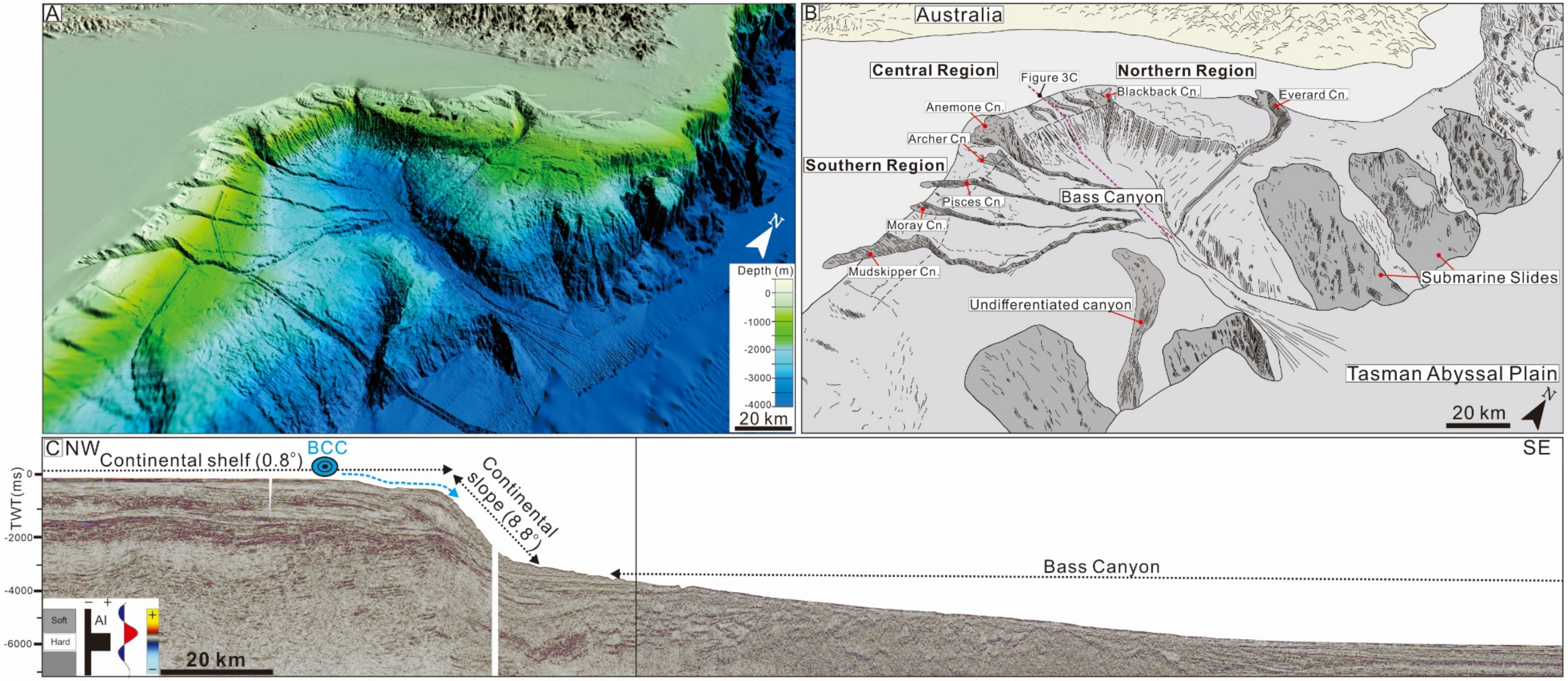

A
Depth (m)
0
-1000
-2000
-3000
-4000
20 km
N
B
Australia
Central Region
Northern Region
Southern Region
Figure 3C
Blackback Cn.
Everard Cn.
Anemone Cn.
Archer Cn.
Pisces Cn.
Moray Cn.
Mudskipper Cn.
Bass Canyon
Undifferentiated canyon
Submarine Slides
Tasman Abyssal Plain
20 km
N
C
NW
SE
Continental shelf (0.8°)
BCC
Continental slope (8.8°)
Bass Canyon
TWT(ms)
0
-2000
-4000
-6000
Soft
Hard
AI
20 km

Figure 4

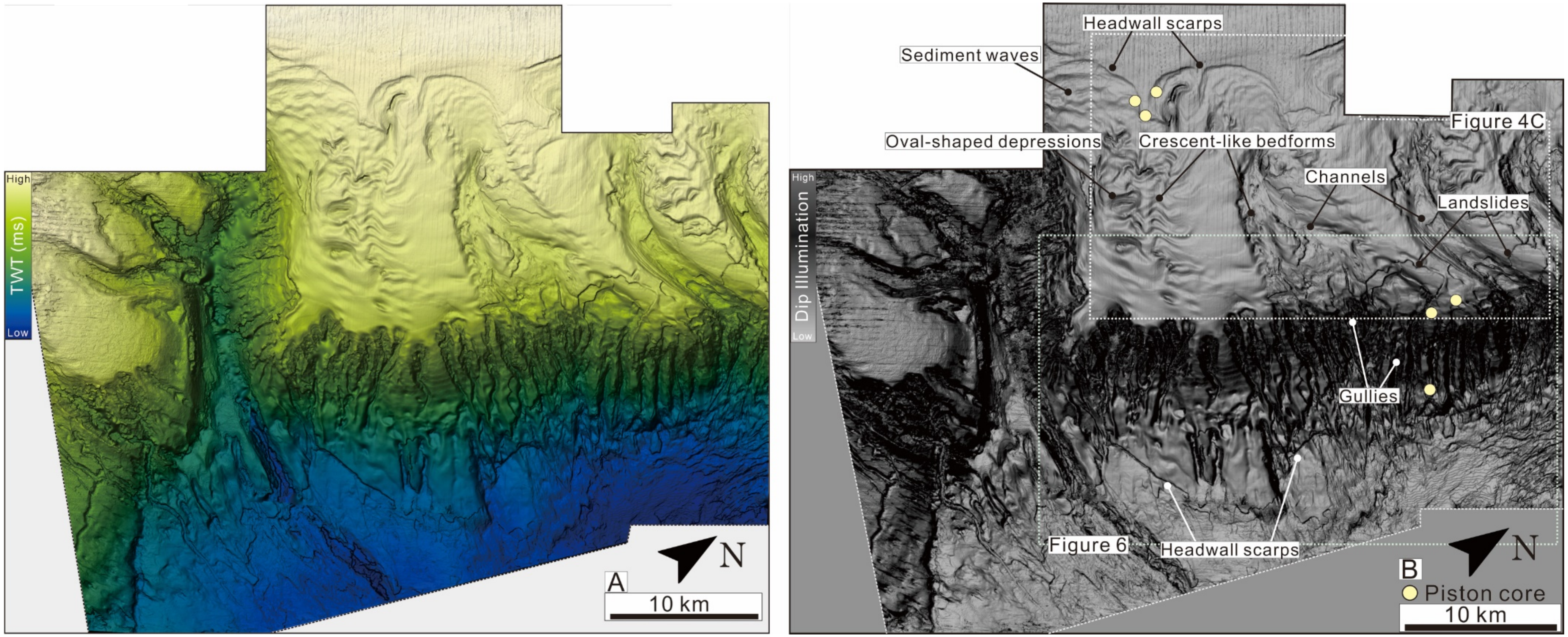

High
TWT (ms)
Low
N
A
10 km
Headwall scarps
Sediment waves
Oval-shaped depressions
Crescent-like bedforms
Figure 4C
Channels
Landslides
High
Dip Illumination
Low
Gullies
Figure 6
Headwall scarps
N
B
Piston core
10 km

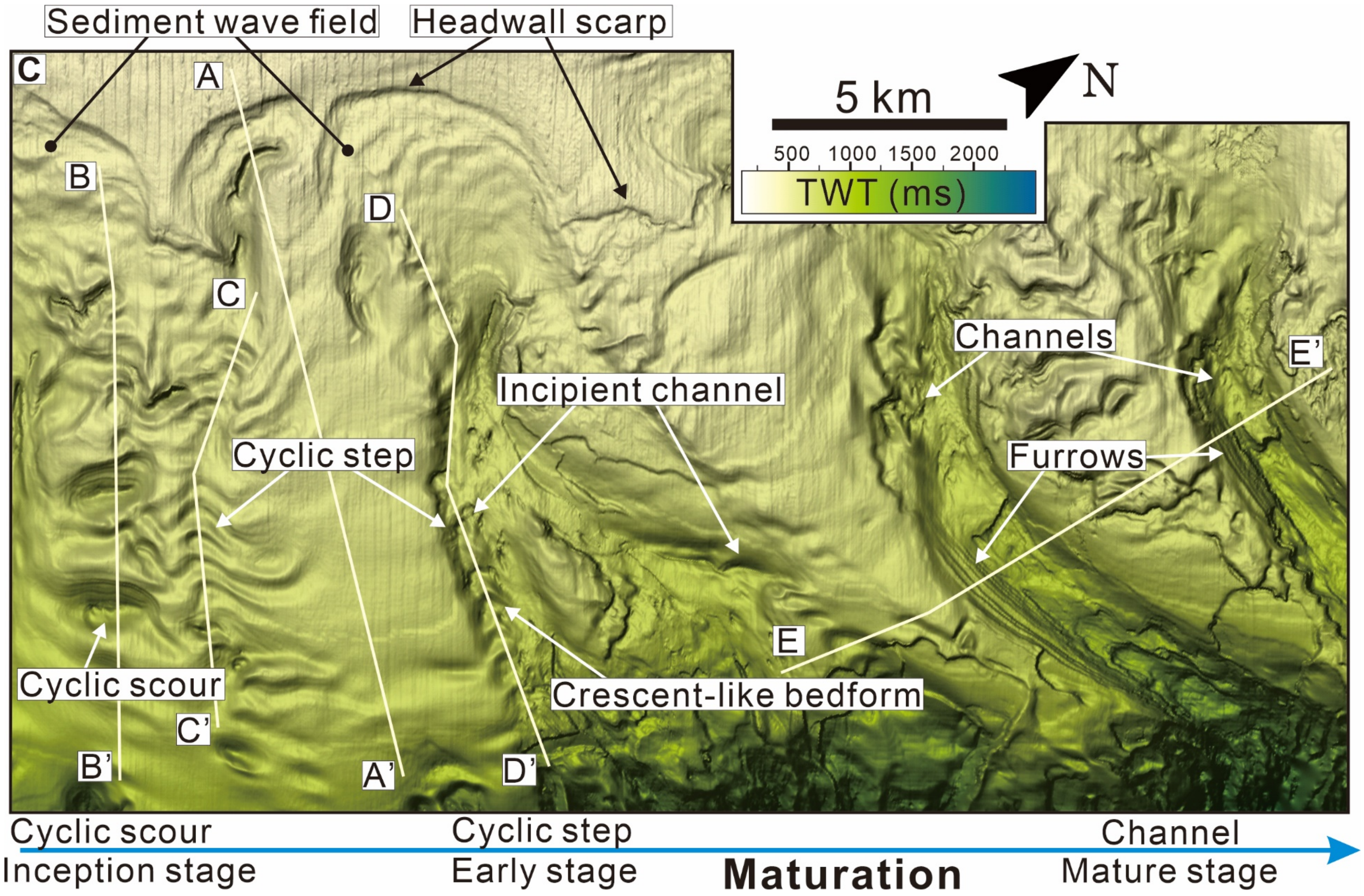
Sediment wave field
Headwall scarp
C
A
B
D
5 km
N
500 1000 1500 2000
TWT (ms)
Channels
E'
Incipient channel
Cyclic step
Furrows
E
Crescent-like bedform
Cyclic scour
C'
B'
A'
D'
Cyclic scour
Inception stage
Cyclic step
Early stage
Maturation
Channel
Mature stage

Figure 5

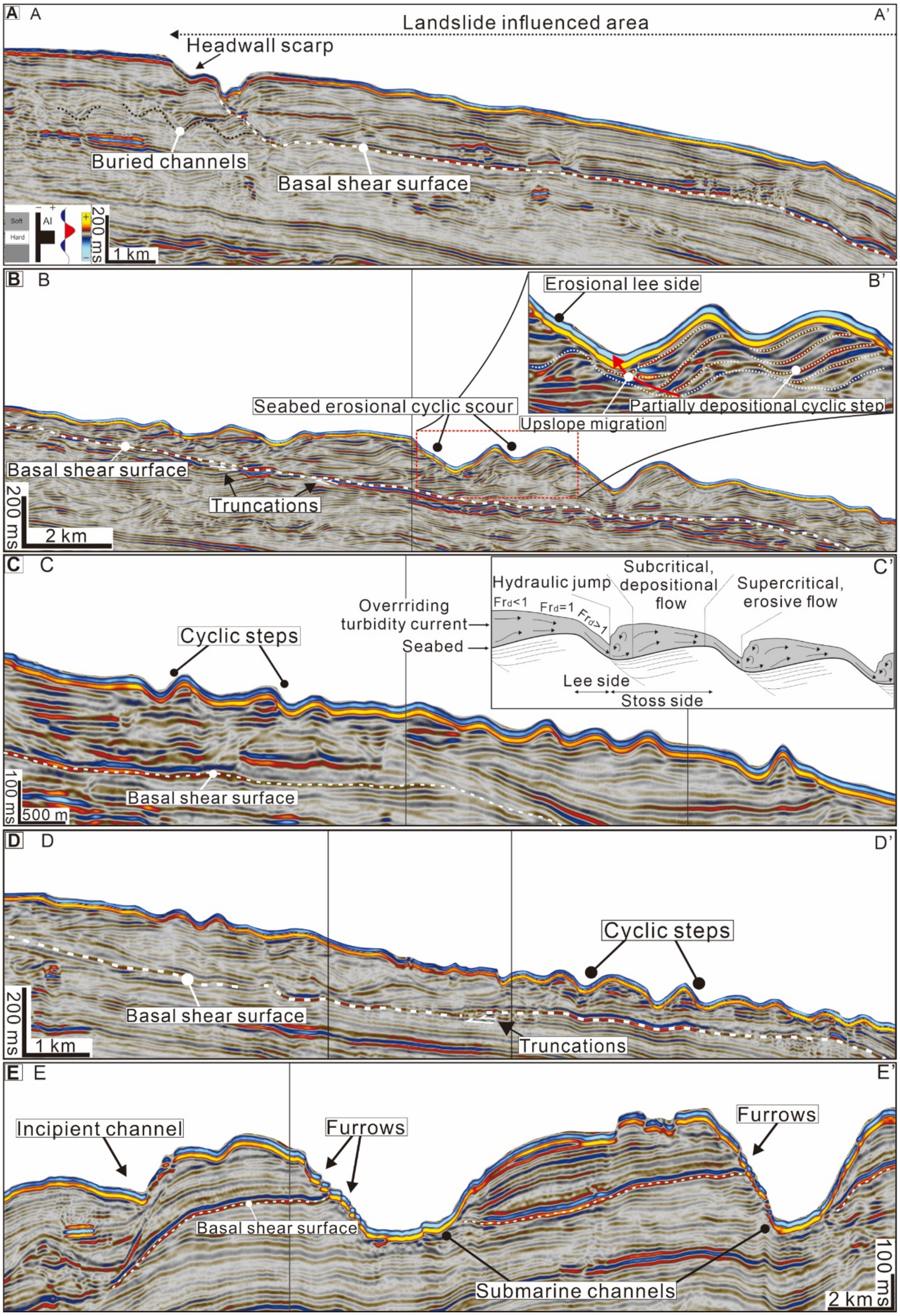
A
A
A'
Landslide influenced area
Headwall scarp
Buried channels
Basal shear surface
Soft
Hard
AI
200 ms
1 km
B
B
B'
Erosional lee side
Seabed erosional cyclic scour
Upslope migration
Partially depositional cyclic step
Basal shear surface
Truncations
200 ms
2 km
C
C
C'
Cyclic steps
Overrriding turbidity current
Seabed
Hydraulic jump
Subcritical, depositional flow
Supercritical, erosive flow
Frd<1
Frd=1
Frd>1
Lee side
Stoss side
Basal shear surface
100 ms
500 m
D
D
D'
Cyclic steps
Basal shear surface
Truncations
200 ms
1 km
E
E
E'
Incipient channel
Furrows
Furrows
Basal shear surface
Submarine channels
100 ms
2 km

Figure 6

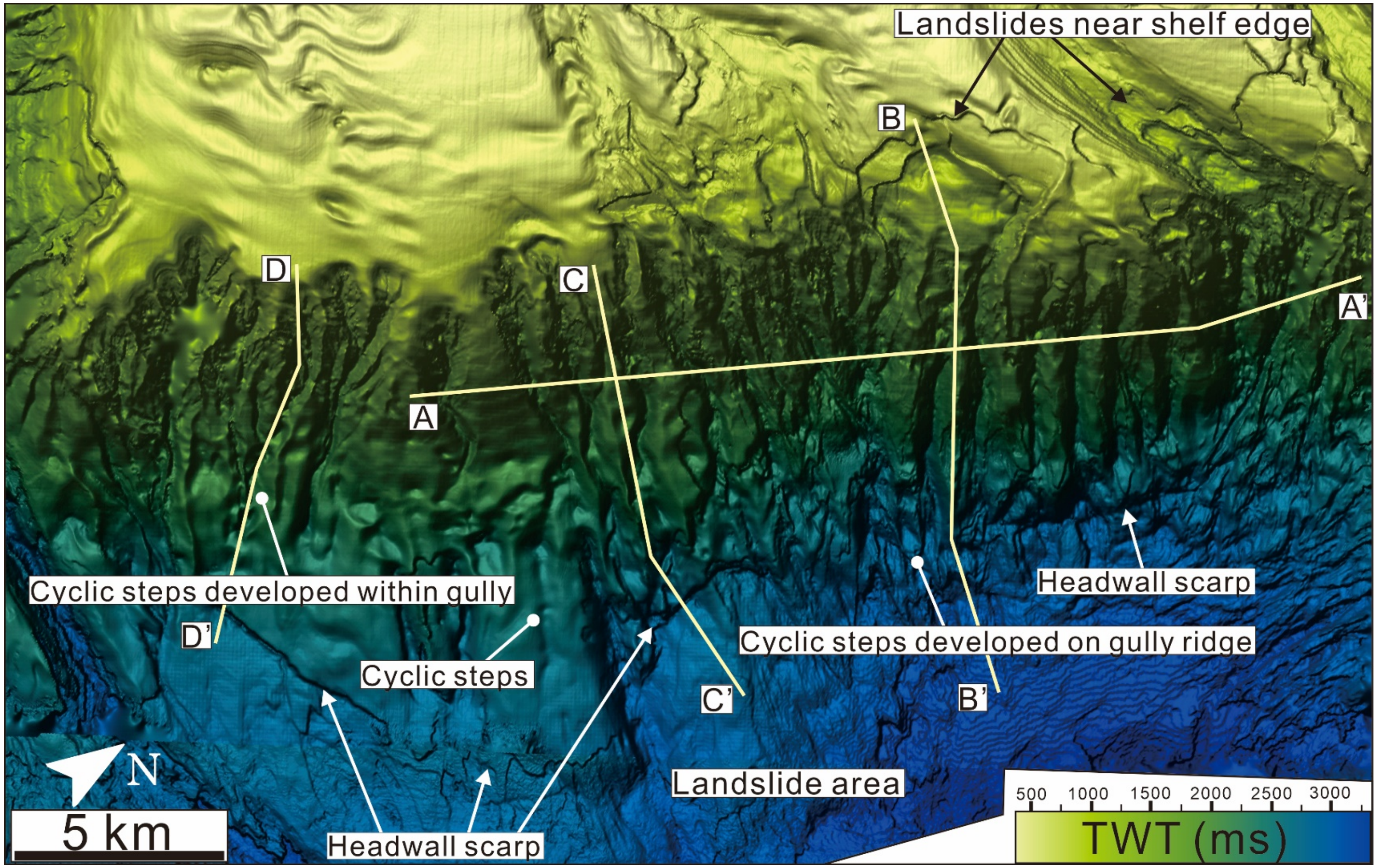

Landslides near shelf edge
B
D
C
A'
A
Upper slope
Lower slope
Headwall scarp
Cyclic steps developed within gully
D'
Cyclic steps
Cyclic steps developed on gully ridge
C'
B'
N
5 km
Headwall scarp
Landslide area
500 1000 1500 2000 2500 3000
TWT (ms)

Figure 7

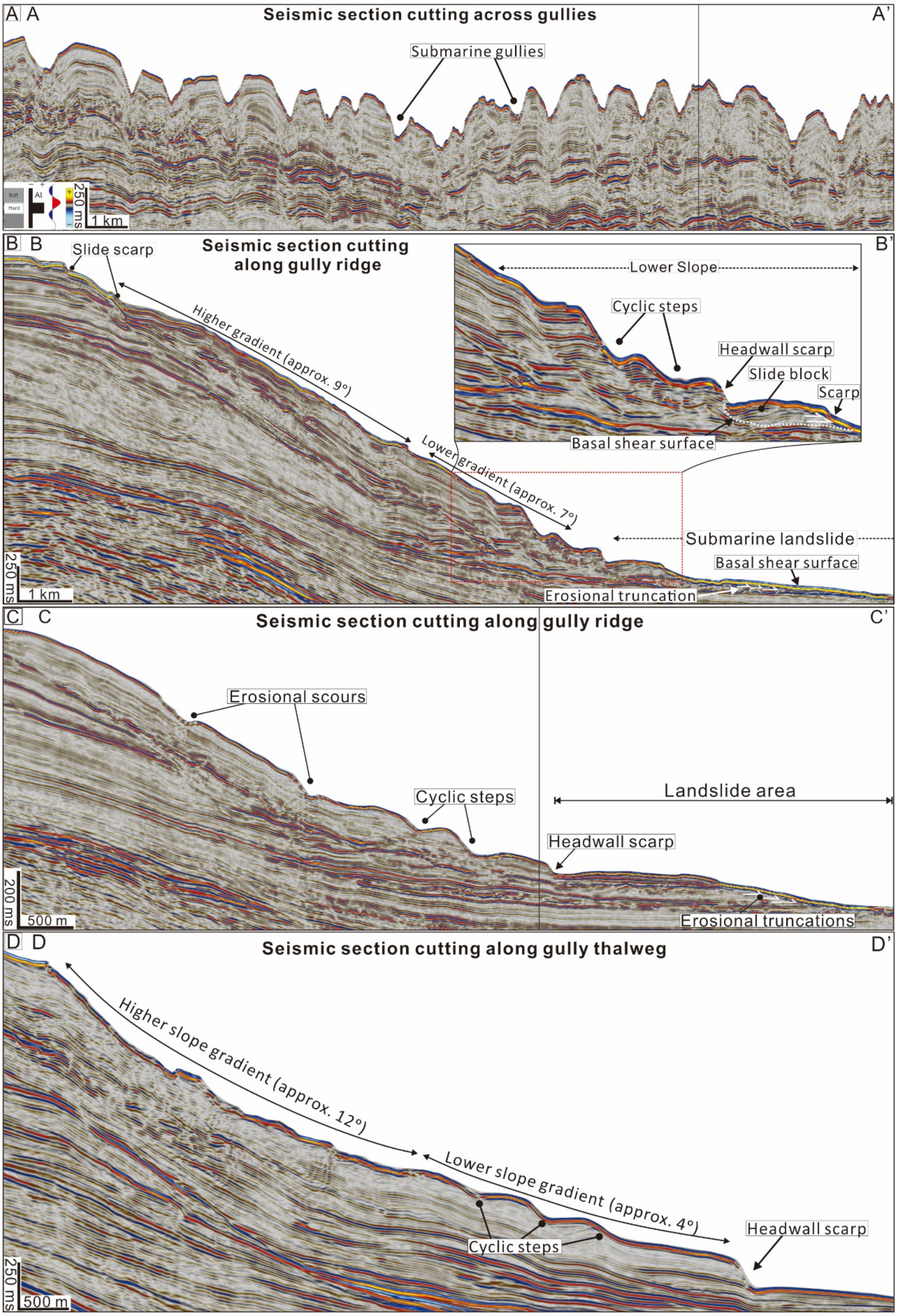
A
A
Seismic section cutting across gullies
A'
Submarine gullies
Soft
Hard
AI
250 ms
1 km
B
B
Slide scarp
Seismic section cutting along gully ridge
B'
Higher gradient (approx. 9°)
Lower gradient (approx. 7°)
Lower Slope
Cyclic steps
Headwall scarp
Slide block
Scarp
Basal shear surface
Submarine landslide
Basal shear surface
Erosional truncation
250 ms
1 km
C
C
Seismic section cutting along gully ridge
C'
Erosional scours
Cyclic steps
Landslide area
Headwall scarp
Erosional truncations
200 ms
500 m
D
D
Seismic section cutting along gully thalweg
D'
Higher slope gradient (approx. 12°)
Lower slope gradient (approx. 4°)
Cyclic steps
Headwall scarp
250 ms
500 m

Figure 8

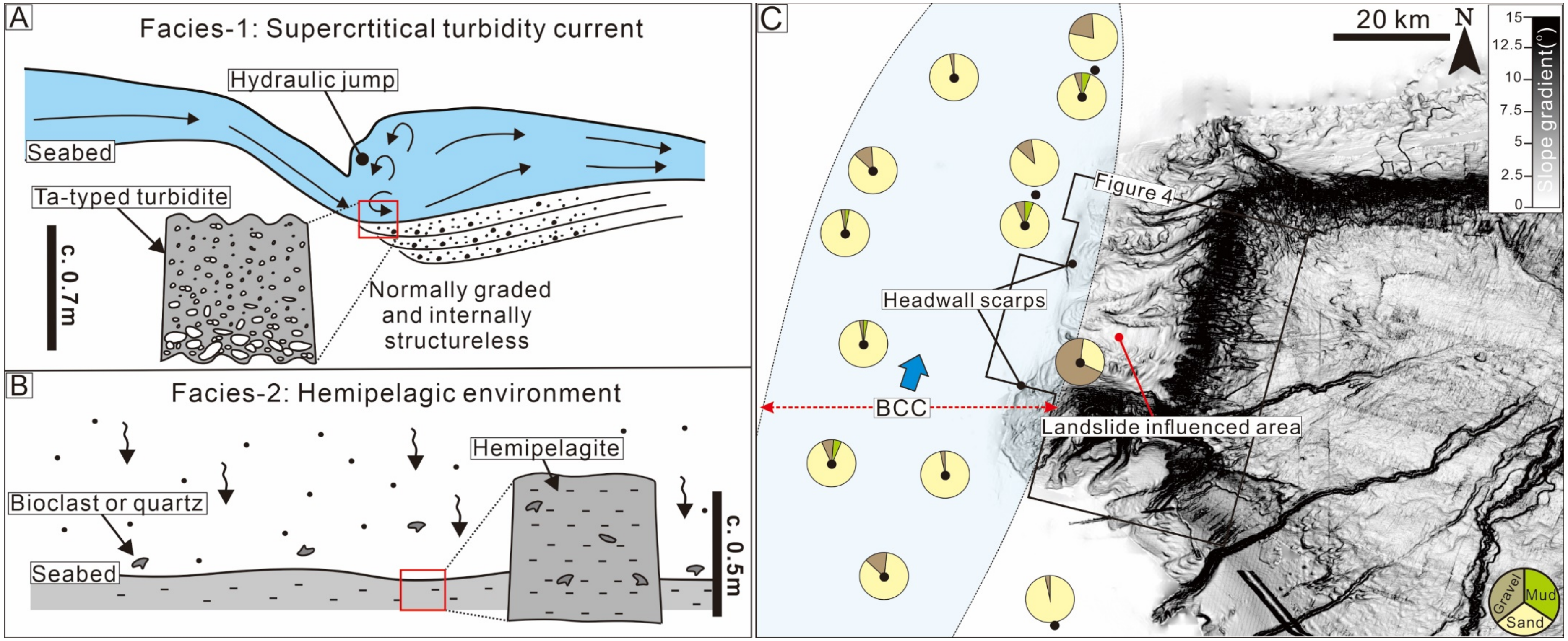

A
Facies-1: Supercrtitical turbidity current
Hydraulic jump
Seabed
Ta-typed turbidite
c. 0.7m
Normally graded
and internally
structureless
B
Facies-2: Hemipelagic environment
Hemipelagite
Bioclast or quartz
Seabed
c. 0.5m
C
20 km
N
15
12.5
10
7.5
5
2.5
0
Slope gradient(°)
Figure 4
Headwall scarps
BCC
Landslide influenced area
Gravel
Mud
Sand

Figure 9

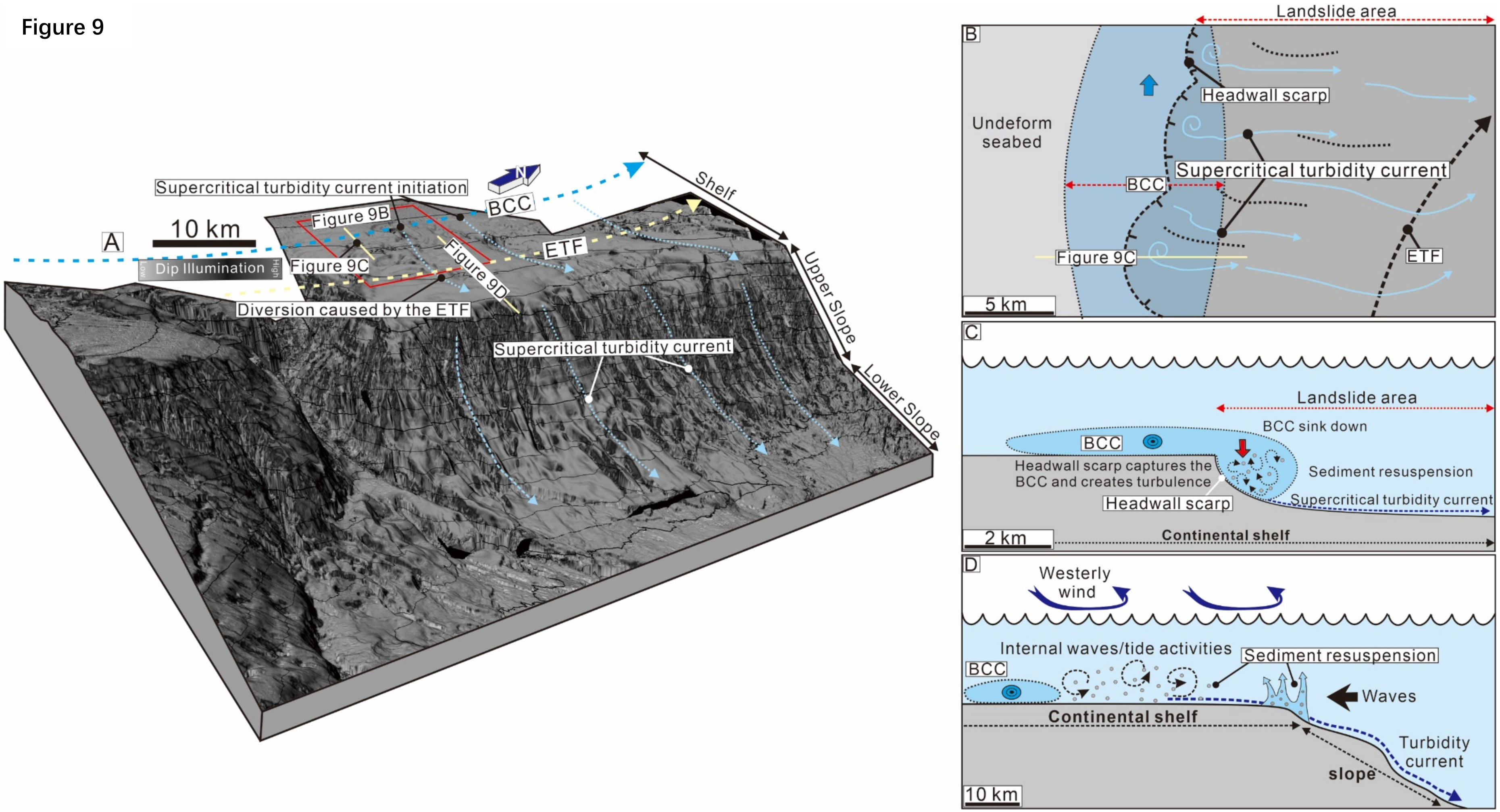

A
10 km
Dip Illumination
Low
High
Supercritical turbidity current initiation
Figure 9B
Figure 9C
Figure 9D
BCC
ETF
N
Shelf
Upper Slope
Lower Slope
Diversion caused by the ETF
Supercritical turbidity current
B
Landslide area
Headwall scarp
Undeform seabed
Supercritical turbidity current
BCC
Figure 9C
ETF
5 km
C
Landslide area
BCC sink down
BCC
Headwall scarp captures the BCC and creates turbulence
Sediment resuspension
Supercritical turbidity current
Headwall scarp
2 km
Continental shelf
D
Westerly wind
Internal waves/tide activities
Sediment resuspension
BCC
Waves
Continental shelf
Turbidity current
slope
10 km

Figure 10

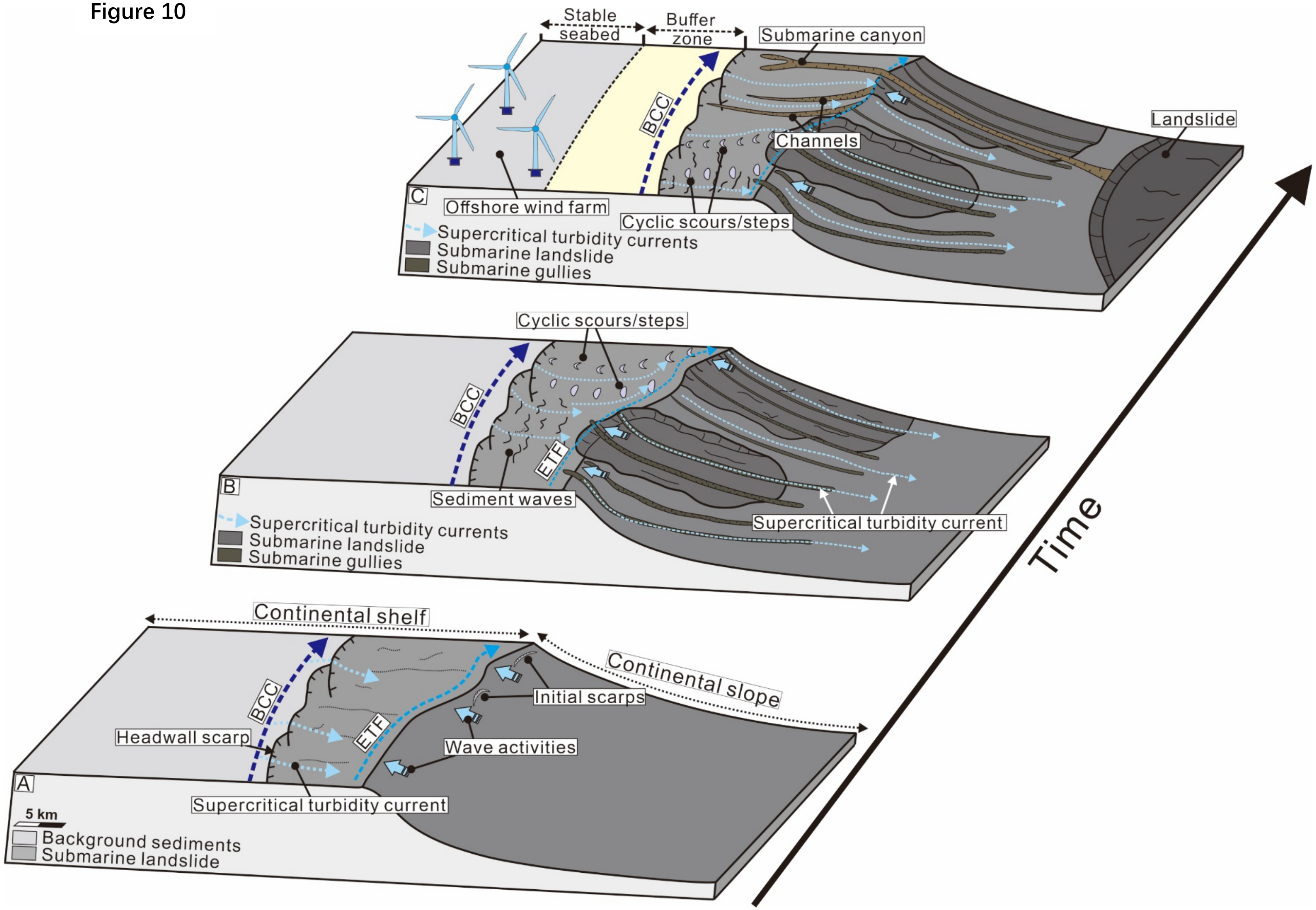
Stable seabed
Buffer zone
Submarine canyon
BCC
Landslide
Channels
Offshore wind farm
Cyclic scours/steps
C
Supercritical turbidity currents
Submarine landslide
Submarine gullies
Cyclic scours/steps
BCC
ETF
B
Sediment waves
Supercritical turbidity current
Supercritical turbidity currents
Submarine landslide
Submarine gullies
Continental shelf
Continental slope
BCC
Initial scarps
ETF
Headwall scarp
Wave activities
A
Supercritical turbidity current
5 km
Background sediments
Submarine landslide
Time